

Supplementary materials

Polymer-clay nanocomposites thermal stability: Experimental evidence of the radical trapping effect.

Hudson W. P. Carvalho^{a,b,‡}, Celso V. Santilli^a, Valérie Briois^b and Sandra H. Pulcinelli^{a*}

^a Institute of Chemistry -UNESP, Rua Prof. Francisco Degni 55, 14800-900, Araraquara, Brazil. ^b Synchrotron SOLEIL, L'Orme des Merisiers, BP 48, 91192 Saint-Aubin, France.

*Present address: Institute for Chemical Technology and Polymer Chemistry, KIT, Engesserstrasse 20, 76131, Karlsruhe, Germany

*sadrap@iq.unesp.br. Phone +55 16 3301 9638.

Experimental Section

Clay chemical composition from VAN OLPHENA and H.; FRIPIAT, J. J.¹

Montmorillonita Arizona (Ari), collected in Country of Apache, Arizona, EUA.

Chemical composition (%): SiO₂(60.4), Al₂O₃(17.6), TiO₂(0.24), Fe₂O₃(1.42), FeO(0.08), MnO(0.099), MgO(6.46), CaO(2.82), Na₂O(0.063), K₂O(0.19), F(0.287), P₂O₅(0.020).

Cationic exchange capacity: 120.0 meq/100 g.

Structural formula: (Ca_{0.39}Na_{0.36}K_{0.02})[Al_{2.71}Mg_{1.11}Fe³⁺_{0.12}Mn_{0.01}Ti_{0.03}][Si_{8.00}]O₂₀(OH)₄.

Iron content: 0.32 at.%

Montmorillonita Wyoming (Wyo), collected in Country of Crook, Wyoming, EUA.

Chemical composition (%): SiO₂(62.9), Al₂O₃(19.6), TiO₂(0.090), Fe₂O₃(3.35), FeO(0.32), MnO(0.006), MgO(3.05), CaO(1.68), Na₂O(1.53), K₂O(0.53), F(0.111), P₂O₅(0.049), S(0.05).

Cationic exchange capacity: 76.4 meq/100 g.

Structural formula: (Ca_{0.12}Na_{0.12}K_{0.15})[Al_{3.01}Fe³⁺_{0.41}Mn_{0.01}Mg_{0.54}Ti_{0.02}][Si_{7.98}Al_{0.02}]O₂₀(OH)₄.

Iron content: 1.02 at.%

c) **Montmorillonita Nontronita** (Non), collected in South Australia, Austrália.

Chemical composition (%): SiO₂(56.99), Al₂O₃(3.4), Fe₂O₃(37.42), MgO(0.34), CaO(2.67), Na₂O(0.11), K₂O(0.02).

Cationic exchange capacity: 69.7 meq/100 g

Structural formula: (Na⁺_{0.97})[Al_{0.52}Fe³⁺_{3.32}Mg_{0.17}][Si_{7.57}Al_{0.01}Fe²⁺_{0.42}]O₂₀(OH)₄.

Iron content: 8.10 at.%

Preparation of PMMA-MMT nanocomposites

Purification of natural clays

The natural clays Arizona (Ari), Wyoming (Wyo) and Nontronite (Non) were kindly supplied by Dr. Emmanuelle Montarges-Pelletier from the Laboratoire Environnement et Minéralurgie, Vandoeuvre-lès-Nancy, France. The first step consisted on the purification of the clay phase from the soil. For this purpose, 20 g of soil were dispersed in a 500 mL of deionized water and then 10 g of NaCl were added. This mixture was stirred up for 24 h and centrifuged at 10,000 rpm for 20 min. The bottom of the precipitate was discarded (sand soil fraction) while the top of the mixture was recovered; this procedure was repeated twice more. Then the precipitate was washed up by redispersion in deionized water, followed by centrifugation; such process can be repeated until the recovery of the swelling of the clay phase.

Organophilization of natural clays

The Na^+ ions were exchanged by dimethyloctadecyl ammonium (C18). Firstly 1.5 g of C18 were dissolved in 100 mL of deionized water. Then 1.5 g of the clay phase were stirred during 24 h in the C18 solution. Afterwards the clay was recovered by centrifugation (10,000 rpm), the precipitate was washed up with deionized water and centrifuged again. The washing procedure was repeated twice and finally, the organophilized clay phase was dried at 60°C for 24h.

Nanocomposite Preparation

The nanocomposites were prepared by *in situ* MMA radical polymerisation in clay THF dispersion. Organophilic clay was dispersed in a flask containing 4.03 mL of THF and maintained for 3 h under 10 kHz ultrasound, then 0.019 mL of MMA was added and the dispersion was kept under magnetic stirring for 24 h. The initiator, 2.10^{-5} mol of benzoyl peroxide, was added and the polymerisation reaction was performed under magnetic stirring at 70°C for 15 h. The resulted suspension was poured into a substrate of polytetrafluoroethylene and dried at room temperature for 24 h and finally dried at 100°C for one hour. The nanocomposites were prepared at nominal loadings of 0.3, 1.0, 3.0 and 6.0 wt. % of organophilic clay.

Characterization

Thermogravimetry

The thermogravimetric analyses were carried out under air flow of $100\text{mL}\cdot\text{min}^{-1}$ and heating rate of $10^\circ\text{C}\cdot\text{min}^{-1}$ and $5^\circ\text{C}\cdot\text{min}^{-1}$, using an SDT Q600TA Instruments.

SAXS

Small angle X-ray scattering patterns were recorded in transmission mode, from solid films in vacuum ambient using a SAXS Nanostar System from Bruker Instruments operating at 1.2 kW. The X-ray was supplied by a Cu anode monochromatized at $\text{CuK}\alpha_1$ wavelength ($\lambda = 0,15418 \text{ nm}$). The point focus geometry X-ray beam was collimated by a Göbel mirror followed by three pinholes. The detector is a filament two dimension Vantec, which was placed 64.8 cm away from the sample in order to record the scattering intensity for scattering vector ranging from 0.1 nm^{-1} to 3.5 nm^{-1} .

Quick-EXAFS

The Fe K X-ray absorption spectra were collected in the Quick-EXAFS mode on the SAMBA beamline at SOLEIL Synchrotron². On this experimental station the white beam is collimated and vertically focused by two Pd-coated silicon cylindrical bendable mirrors. The beam is monochromatized by a Si (111) double crystal channel cut. The oscillation frequency of the channel-cut was set to 1 Hz, corresponding to the acquisition of two spectra every 1s. Only the set of spectra recorded with increasing Bragg angle was considered in the analysis. Data were recorded in transmission mode and the X-ray attenuation measured by ionization chambers with nitrogen filling gas. For improving the signal to noise ratio, the data collected at Room Temperature were averaged over 150 spectra (2.5 min). The samples were placed into a home-made oven³ and heated under air atmosphere from room temperature until 450°C at $5^\circ\text{C}.\text{min}^{-1}$. 10 strictly superimposable successive spectra were collected during the thermal decomposition, indicating that no significant local order change occurs. They were merged to be used as one temperature point in the subsequent data analysis. The change in temperature occurring during this 10 s is only of 0.8°C .

EXAFS and XANES data analysis:

The analysis of the X-ray absorption data was carried out using the software package Athena and Artemis⁴. For the XANES analysis, a linear background was fitted to the pre-edge region and subtracted from the spectra which were normalized in a consistent way. Data were calibrated in energy using the maximum of the first derivative of a metallic iron reference foil recorded simultaneously with the data related to the samples. For the EXAFS analysis, first a pre-edge background was removed using a linear function. A post-edge background using the ‘Autobk’ algorithm was applied with a cut-off $R_{\text{bkg}} = 1$ and k-weight = 2 in order to isolate the EXAFS oscillations $\chi(k)$. Then the EXAFS data were Fourier transformed using a k^3 -weighting Kaiser-Bessel window. EXAFS fitting of distances and Debye-Waller factors were performed with the ARTEMIS interface to IFEFFIT⁵ using least-square refinements. The S_0^2 amplitude reduction parameter which takes multielectronic effects into account and the energy shift E_0 were first calibrated by fitting relevant crystalline references. The reliability of the fit was assessed by a residual factor R_F that was minimized.

Results

Figure S1 presents the imaginary part of the backward Fourier transforms of the EXAFS spectra of the pristine clays Arizona, Wyoming and Nontronite. The Figure S1 shows the experimental data and the respective refinements obtained with the structural parameters presented in Table S1.

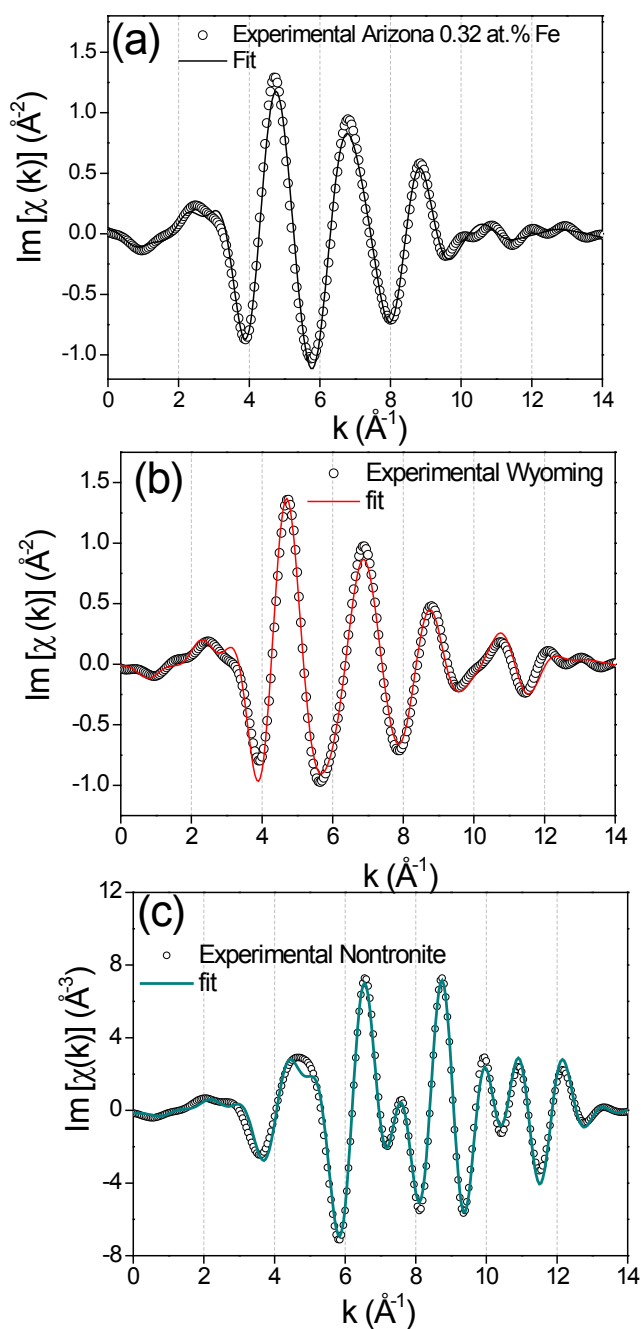


Figure S1. Imaginary part of the backward Fourier transformation of the experimental and fitted spectra of pristine clays at room temperature; (a) Arizona 0.32 at.% of Fe, (b) Wyoming 1.02 at.% of Fe and (c) Nontronite 8.10 at.% of Fe.

Table S1. Structural parameters determined from EXAFS data analysis of pristine clays at room temperature.

| Sample | Shell | Atom | N | R (Å) | σ^2 (10 ⁻³ Å ²) | ρ (%) |
|---------------------|-----------------|--------|------------------|-------------------|-----------------------------------------------|------------|
| Pristine Nontronite | 1 st | O | 6 ^c | 2,01 ^f | 5 ^f | 1,7 |
| | 2 nd | Fe-Oct | 2,4 ^f | 3,09 ^f | 3 ^f | |
| | 2 nd | Al-Oct | 0,6 ^f | 2,92 ^f | 3 ^f | |
| Pristine Arizona | 1 st | O | 6 ^c | 1,98 ^f | 4,9 ^f | 5.4 |
| | 2 nd | Fe-Oct | 2 ^c | 3,01 ^f | 4,0 ^f | |
| | 2 nd | Al-Oct | 1 ^c | 3,00 ^f | 4,7 ^f | |
| Pristine Wyoming | 1 st | O | 6 ^c | 1,99 ^f | 5,3 ^f | 2.3 |
| | 2 nd | Al-Oct | 3 ^c | 3,00 ^f | 5,7 ^f | |
| | 3 rd | Si-Tet | 4 ^c | 3,19 ^f | 10 ^f | |

f- fitted parameter, c- constrained parameter, $S_0^2 = 0.9$, ΔE_0 Nontronite= 3.29 eV, ΔE_0 Wyoming = 1.5 ± 3.9eV, ΔE_0 Arizona = 2.4 ± 1.5 eV.

Figure S2 shows SAXS curves of organoclays and their PMMA-MMT nanocomposites. The shift to low q-range of the first and second harmonic of diffraction peaks of nanocomposite scattering curves evidences the intercalated structure. The basal distances of clays after PMMA intercalation were determined from the position of those peaks and d_{001} values slightly depends on the clay chemical composition ($d_{001} = 39.8\text{ \AA}$ for PMMA-Arizona and $d_{001}=37.2\text{ \AA}$ for both PMMA-Wyoming and PMMA-Nontronite). Usually the basal distance of sodium MMT clays varies between 10 to 12 Å.

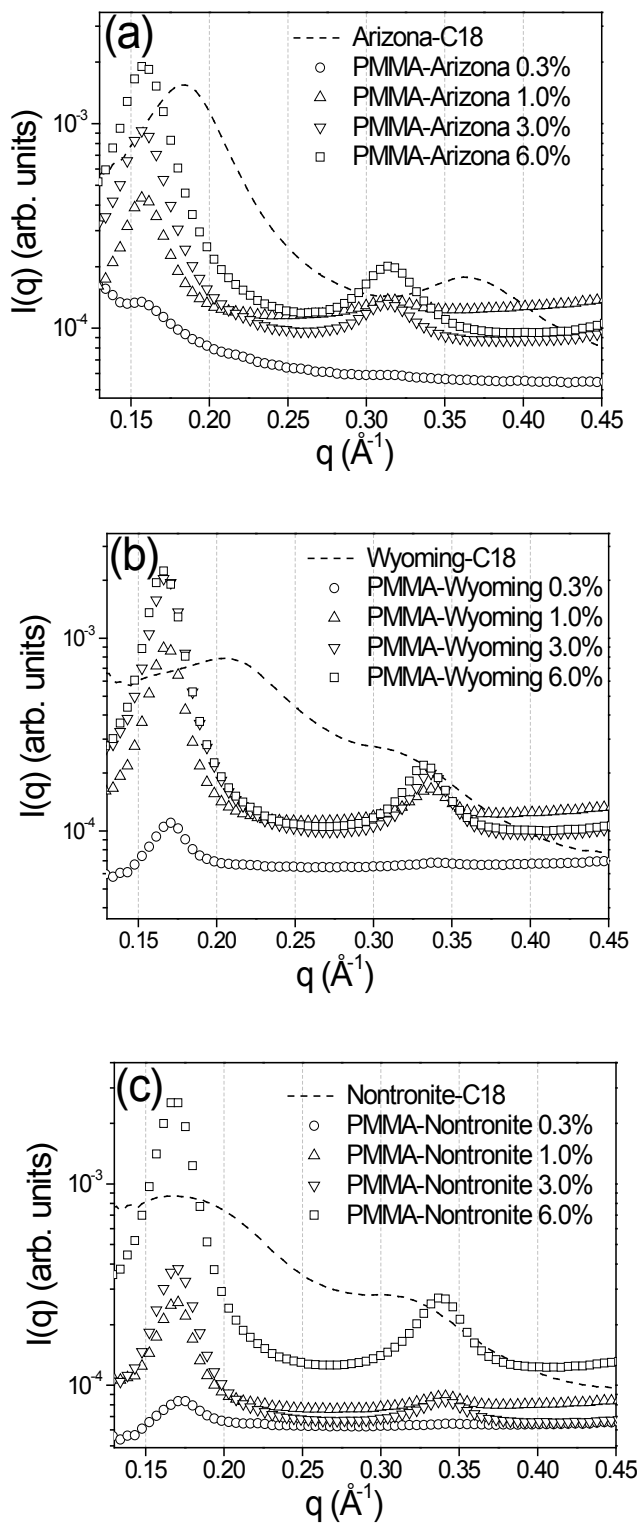


Figure S2. SAXS curves of organic clays and respective PMMA-MMT nanocomposites obtained with (a) Arizona 0.32 at.% of Fe, (b) Wyoming 1.02 at.% of Fe and (c) Nontronite 8.10 at.% of Fe.

Figure S3 presents the thermogravimetric analysis, under dynamic air atmosphere, heating rate of $10^{\circ}\text{C min}^{-1}$. For a given clay, the thermal stability of the nanocomposites increases as a function of the clay loading. In the same way, for a given clay loading of different clays, the thermal stability increases as function of the Fe ion content.

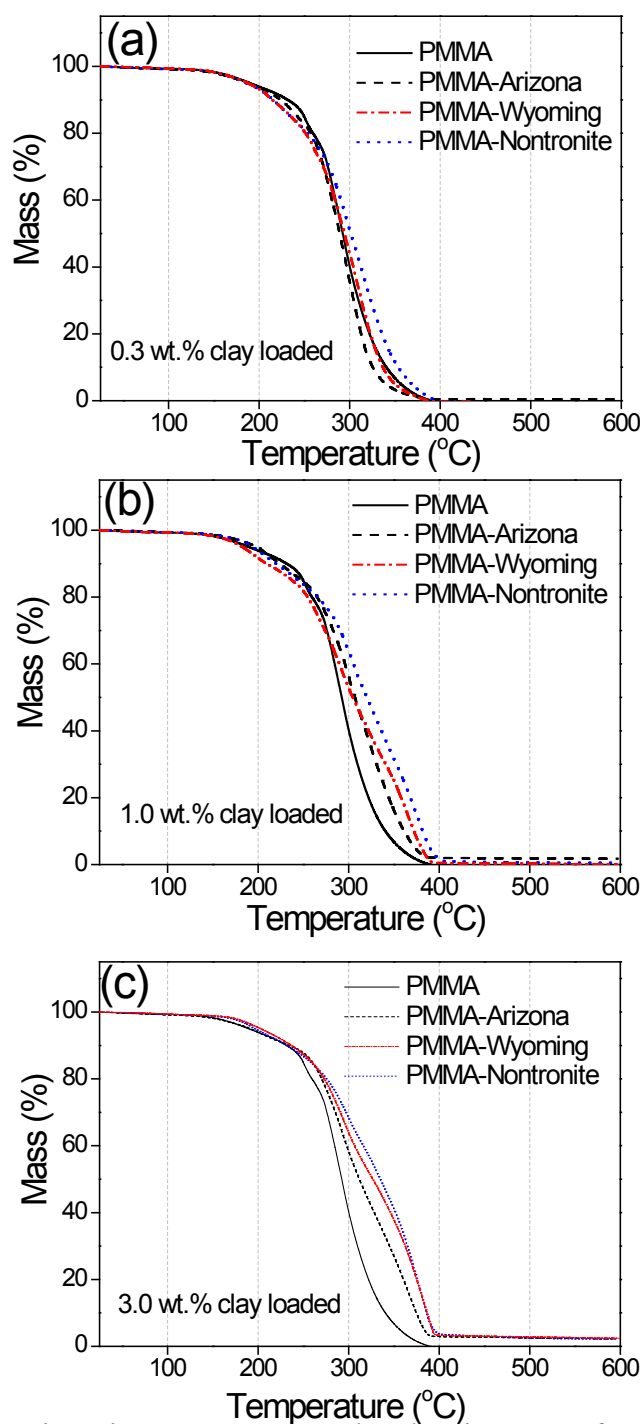


Figure S3. Thermogravimetric curves measured at heating rate of $10^{\circ}\text{C min}^{-1}$ for PMMA-MMT nanocomposites prepared with Arizona 0.32 at.% of Fe, Wyoming 1.02 at.% of Fe and Nontronite 8.10 at.% of Fe.

Table S2. Structural parameters fitted from EXAFS spectra of nanocomposite PMMA-Nontronite 6 at.%, at 450°C during thermal degradation and at 50°C after residue cooling.

| Sample | Edge | Shell | At | N | r (\AA) | $\sigma (10^{-3} \text{\AA}^2)$ | $\rho (\%)$ |
|------------------------------------|------|-----------------|----|----------------|--------------------|---------------------------------|-------------|
| PMMA-Nontronite 6% 450°C | Fe | 1 st | O | 6 ^c | 2,07 ^f | 22,7 ^f | 4,6 |
| PMMA-Nontronite 6% residue 50°C | | 1 st | O | 6 ^c | 1,99 ^f | 11,3 ^f | 2,4 |

^f- fitted parameter; ^c- constrained parameter

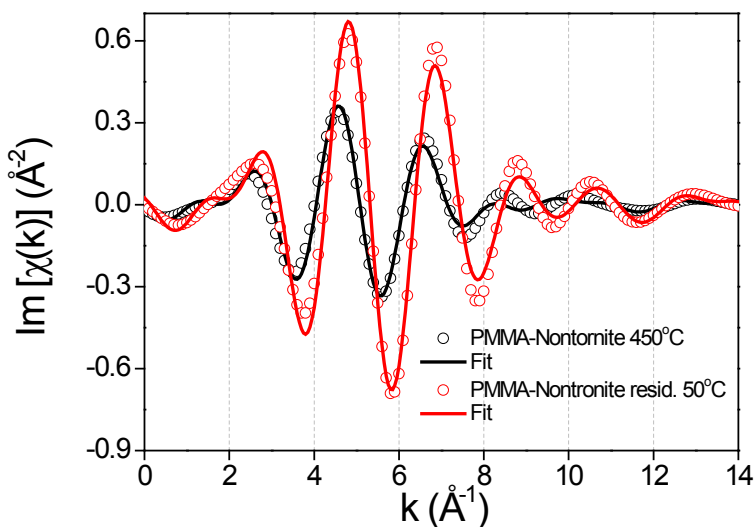


Figure S4. Imaginary part of the backward Fourier transformation of the experimental and fitted spectra of PMMA-Nontronite 6 wt.% loaded nanocomposite at 450°C and at 50°C after cooling down the residue. Experimental and fitted data. Nontronite clay contains 8.10 at.% of Fe.

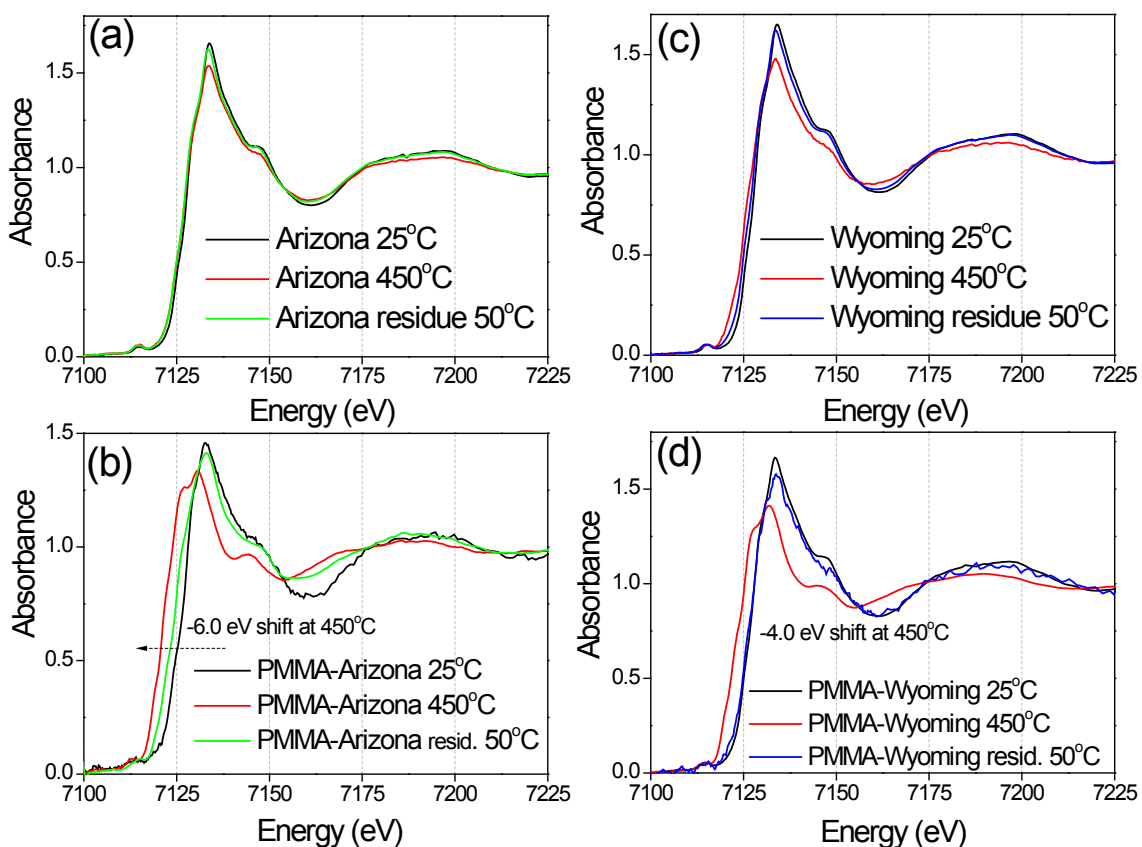


Figure S5. In situ XAS spectra at room temperature, at 450°C and after cooling down the residue of the pristine clay and the respective PMMA-MMT nanocomposites, under air atmosphere: (a) pristine Arizona clay, (b) PMMA-Arizona 6 wt.% loaded nanocomposite, (c) pristine Wyoming clay and (d) PMMA-Wyoming 6 wt.% loaded nanocomposite. Arizona 0.32 at.% of Fe and Wyoming 1.02 at.% of Fe.

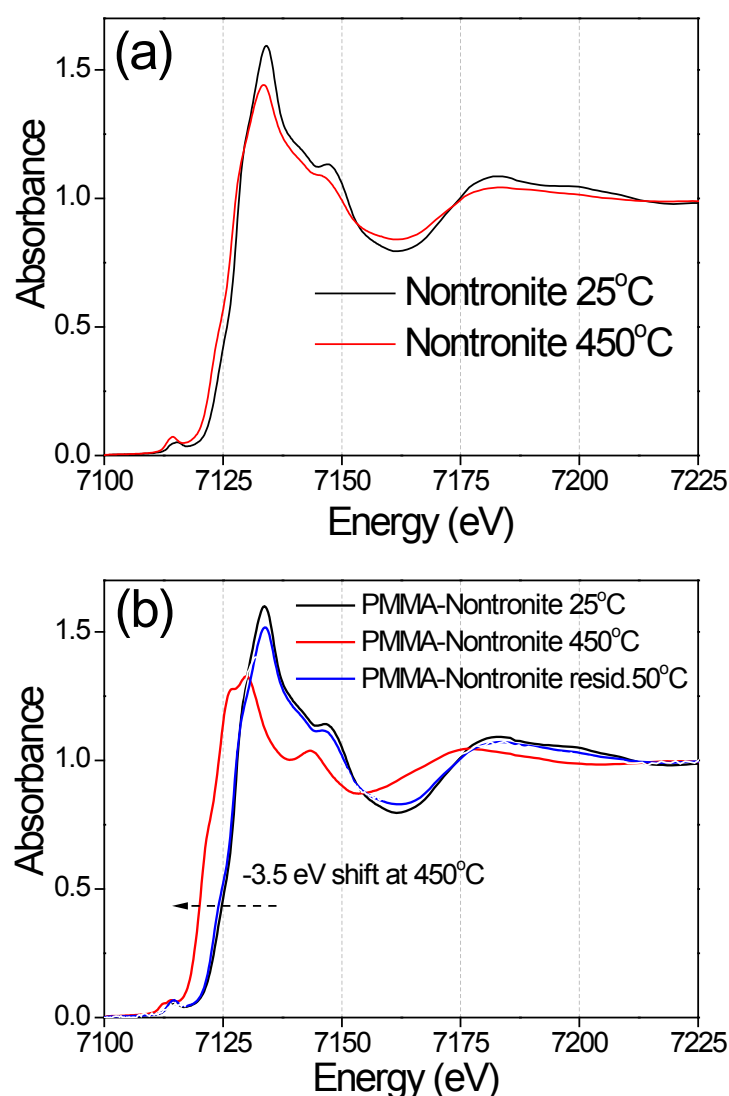


Figure S6. In situ XAS spectra at room temperature, at 450°C and after cooling the residue of the pristine clay and respective PMMA-MMT nanocomposites, under air atmosphere: (a) pristine Nontronite clay, (b) PMMA-Nontronite 6 wt.% loaded nanocomposite. Nontronite clay contains 8.10 at.% of Fe

References

1. H. Van Olphen and J. J. Fripiat, *Data Handbook for Clay Minerals and Other Non-metallic Minerals*, Pergamon Press, Oxford, 1979.
2. E. Fonda, A. Rochet, M. Ribbens, L. Barthe, S. Belin and V. Briois, *J. Synchrotron Radiat.*, 2012, **19**, 417.
3. C. La Fontaine, L. Barthe, A. Rochet and V. Briois, *Catal. Today*, 2013, **205**, 148.
4. B. Ravel and M. Newville, *J. Synchrotron Radiat.*, 2005, **12**, 537.
5. M. Newville, *J. Synchrotron Radiat.*, 2001, **8**, 322.